

Comparison of Simulated and Observed Continental Tropical Anvil Clouds and Their Radiative Heating Profiles

SCOTT W. POWELL AND ROBERT A. HOUZE JR.

Department of Atmospheric Sciences, University of Washington, Seattle, Washington

ANIL KUMAR

Hydrological Science Branch, NASA Goddard Space Flight Center, Greenbelt, and Earth System Science Interdisciplinary Center, University of Maryland, College Park, College Park, Maryland

SALLY A. MCFARLANE

Climate Physics Group, Pacific Northwest National Laboratory, Richland, Washington

(Manuscript received 16 September 2011, in final form 19 April 2012)

ABSTRACT

Vertically pointing millimeter-wavelength radar observations of anvil clouds extending from mesoscale convective systems (MCSs) that pass over an Atmospheric Radiation Measurement Program (ARM) field site in Niamey, Niger, are compared to anvil structures generated by the Weather Research and Forecasting (WRF) mesoscale model using six different microphysical schemes. The radar data provide the statistical distribution of the radar reflectivity values as a function of height and anvil thickness. These statistics are compared to the statistics of the modeled anvil cloud reflectivity at all altitudes. Requiring the model to be statistically accurate at all altitudes is a stringent test of the model performance. The typical vertical profile of radiative heating in the anvil clouds is computed from the radar observations. Variability of anvil structures from the different microphysical schemes provides an estimate of the inherent uncertainty in anvil radiative heating profiles. All schemes underestimate the optical thickness of thin anvils and cirrus, resulting in a bias of excessive net anvil heating in all of the simulations.

1. Introduction

Impacts of clouds on radiative heating and the atmospheric general circulation remain a great uncertainty in attempts to model future climate (Solomon et al. 2007; Dufresne and Bony 2008). In the tropics, a large amount of total upper-level ice cloud originates from anvil cloud that extends from precipitating deep convection (Yuan and Hartmann 2008; Yuan and Houze 2010). Much of the deep convection in the tropics is associated with mesoscale convective systems (MCSs), which occur when cumulonimbus clouds organize into a cloud system up to several hundred kilometers in dimension (Houze 2004). Well-developed MCSs typically encompass a large area

of stratiform precipitation, a smaller but more intense region of convective towers, and a cirrus anvil extending laterally in the upper troposphere from the deeply convective or stratiform regions of MCSs (Houze et al. 1989). While the precipitating portion of the MCS may dissipate, ice clouds formed from the anvil may persist for several more hours or days. The MCS structure produces a latent heating profile with a maximum in the upper troposphere (Houze 1982), which impacts the general circulation of the tropics (Hartmann et al. 1984; Schumacher et al. 2004; Lin et al. 2004). The bias of net heating toward the upper troposphere caused by latent heating in the stratiform regions is reinforced by convergence of longwave and shortwave radiative fluxes aloft in the anvil cloud (Houze 1982; see his Fig. 12). Anvil clouds are also important agents for transferring moisture to the upper troposphere since they eventually evaporate and leave unprecipitated water aloft. Therefore, because of their resulting effects on heating and

Corresponding author address: Scott W. Powell, Department of Atmospheric Sciences, University of Washington, Box 351640, Seattle, WA 98195.
E-mail: spowell@atmos.uw.edu

moistening of the atmosphere, MCSs must be accurately parameterized—if not explicitly resolved—in global models.

Adjustments in a microphysics scheme may significantly change a model's representation of upper-level clouds. Clement and Soden (2005) showed that a general circulation model (GCM) was sensitive to microphysical processes through which MCSs produce anvil cloud. Specifically, they increased the precipitation efficiency—defined as the fraction of total convective condensate converted to rainfall—from 99% to 99.5% in their parameterization. This small increase reduced formation of high cirrus clouds and substantially altered radiative heating in the upper troposphere. Since precipitation efficiency is related to how much convectively generated ice can be stored in the anvil, we require better understanding of anvil cloud generation in order to confidently determine radiative heating profiles associated with convectively generated ice clouds.

Other recent studies have made attempts to simulate tropical clouds using cloud-resolving models and compared the simulations to three-dimensional satellite and radar observations (Blossey et al. 2007; McFarlane et al. 2007; Zeng et al. 2008; Lopez et al. 2009; Matsui et al. 2009). Thin cirrus clouds and anvil clouds are often misrepresented as too optically thin and infrequent, and the range of simulated reflectivities in such clouds is too large at all heights. Improvements to the accuracy of the large-scale forcing or ice microphysics or changes in grid size and resolution may enhance the representation of anvil clouds in models. Several of the studies propose that use of a two-moment microphysical scheme—one that predicts both the number concentration and mixing ratio of cloud and precipitation hydrometeors—may be necessary to accurately parameterize tropical cloudiness.

Given the importance of anvil clouds in the general circulation and climate of the tropics, we seek to determine how well models can represent real anvil clouds by systematically comparing model-simulated anvil clouds with observed anvils. We turn to observations in West Africa, an area noted for frequent, well-defined, westward-propagating MCSs (Hamilton and Archibold 1945; Aspliden et al. 1976; Fortune 1980; Chong et al. 1987; Fink and Reiner 2003; Schumacher and Houze 2006; Futyán and Del Genio 2007). Several prior radar and aircraft studies have documented the anvil cloud properties of West African MCSs (Cetrone and Houze 2009, 2011, hereafter CH09 and CH11; Chong 2010; Protat et al. 2010; Yuan et al. 2011; Frey et al. 2011). Most of these studies are based on data collected near Niamey, Niger (13.477°N, 2.176°E), as part of the African Monsoon Multidisciplinary Analysis (AMMA) during the summer of 2006 (Redelsperger et al. 2006). In particular, the anvils of the

MCSs passing over Niamey were observed by vertically pointing cloud radar; CH09 and CH11 provided statistics of the reflectivity distribution in MCS anvils. However, no previous study has yet characterized radiative heating within these MCS anvil clouds. In this paper, we use the extensive AMMA radar dataset to validate model simulations of MCSs that passed over Niamey, and we use the model output to address the following questions:

- 1) What types of ice hydrometeors are transported to the anvil?
- 2) What is the typical radiative heating profile in anvil clouds?
- 3) Can the model, using any of a variety of microphysical schemes, reproduce realistic MCS anvil?
- 4) How do anvil height and ice water content depend on which microphysical scheme is used?
- 5) Can radiative heating in anvil clouds be accurately portrayed by a model, given cloud properties produced by a microphysical scheme?

The AMMA radar dataset is particularly well suited for the goals of this paper. We require the model to reproduce the statistics of anvil radar echo as a function of both altitude and intensity of reflectivity. Such an approach is a much more thorough test of model performance than comparisons to total precipitation or cloud fraction because a model could more easily produce a reasonable representation of either without replicating realistic cloud structures. However, obtaining an appropriate distribution of anvil reflectivity without essentially correct dynamics and microphysics is likely much more difficult. Our stringent test of the model is thus more likely to require that the anvil cloud be simulated for the right physical reasons. Thus, if such a rigorous testing method replicates correct anvil structures, the model will also provide important insight into the processes involved in anvil formation and maintenance and other physical processes connected with MCSs. Greater understanding of anvil processes will advance development of parameterizations or explicit representations of anvil clouds and thin cirrus in general circulation and climate models.

2. Model description

We use a high-resolution weather forecasting model, version 3.3 of the Weather Research and Forecasting Model (WRF) (Skamarock et al. 2008), to simulate three MCSs that passed over Niamey on 19 July, 11 August, and 8 September 2006. Boundary and initial conditions for the large-scale atmospheric fields, soil moisture and temperature parameters, and sea surface temperature are given by the $1^\circ \times 1^\circ$ 6-hourly National

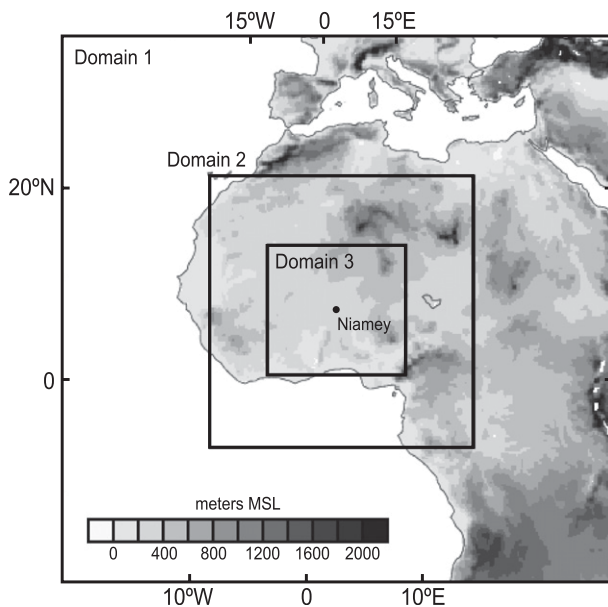


FIG. 1. Domains used in our WRF simulations centered over Niamey, Niger. Grayscale shading indicates the height of surface terrain. The domain consists of an outer region with 27-km horizontal resolution and 300×300 grid points, a nested domain of 9-km resolution with 433×433 grid points, and an inner domain with 3-km resolution and 630×630 grid points.

Centers for Environmental Prediction (NCEP) global final analysis data available online (at <http://dss.ucar.edu/datasets/ds083.2/>). The forcing data are interpolated to the WRF grid using the WRF preprocessing system. The model domain, shown in Fig. 1, consists of an outer domain with 27-km horizontal resolution and 300×300 grid points, a nested domain of 9-km resolution with 433×433 grid points, and an inner domain with 3-km resolution and 630×630 grid points. We examine only anvil clouds that develop and are located within the inner domain. The model has 61 vertical levels equally spaced in WRF coordinates η ($\eta = p_h/p_{hs}$, where p_h is hydrostatic pressure and p_{hs} is surface hydrostatic pressure). The domain ranges in altitude from the surface to approximately 20 km. We employ the Yonsei University (YSU) planetary boundary layer parameterization (Noh et al. 2003; Hong et al. 2006) as well as the Noah land surface model (Ek et al. 2003). For computation of radiative parameters, we use the Rapid Radiative Transfer Model (RRTM; Mlawer et al. 1997; Iacono et al. 2000) long-wave scheme and Dudhia shortwave scheme (Dudhia 1989). The RRTM treats model snow and ice as ice particles, and optical properties of ice clouds are calculated for each spectral band (Fu et al. 1998). Convection is explicitly resolved in the inner domain; however, we use the Kain–Fritsch cumulus parameterization (Kain 2004) in the two larger domains. Simulations were initialized

about 6 h prior to the time that the leading anvil and squall line passed over Niamey. The 19 July and 11 August cases were run for 24 h, and the 8 September case was run for 30 h. An initialization period of 6 h, during which time no data are analyzed, was required so that the model generates an MCS with a distinct squall line and anvil field. After this period, model output was used only every 3 h to avoid repetitive sampling of the same anvil.

Our simulations differ only in the microphysics scheme employed. We test six microphysical schemes for each of three cases simulated. Table 1 provides some characteristics of each parameterization. The Goddard scheme is based on the Purdue–Lin (Lin et al. 1983, hereafter L83) and Rutledge and Hobbs (1984, hereafter RH84) schemes, adds adjustments for ice and water saturation, and eliminates dry growth of graupel. The State University of New York at Stony Brook bulk microphysical parameterization (SBU-YLIN) is a four-class hydrometeor, two-class ice scheme developed from L83 and RH84 that uses the same saturation adjustment used in the Goddard scheme. In addition, it attempts to parameterize the amount of riming that occurs on precipitating ice in order to improve its mass–dimensional relationship of ice particles. The WRF Double-Moment 6-Class Scheme (WDM6) has a flexible size distribution of rain, which is modulated with different microphysical processes according to precipitation type and characteristic of convection. Ice microphysics are based on L83 and RH84 with additional simplification of ice processes described by Dudhia (1989). All other microphysical schemes are relatively new schemes that predict both mixing ratios of one or more frozen hydrometeor classes as well as their number concentrations. The Thompson scheme predicts two moments for ice only and includes very efficient conversion of cloud ice to snow. The Morrison scheme is two-moment for all hydrometeor classes except cloud water. The Milbrandt scheme is two-moment for all hydrometeor classes and adds hail as a fourth class of ice.

3. Radar observations of anvils

The Atmospheric Radiation Measurement Program (ARM) W-band vertically pointing cloud radar (WACR; Mead and Widener 2005) located at the Niamey ARM Mobile Facility (AMF) during AMMA directly observes nonprecipitating or lightly precipitating clouds. Its temporal resolution is 2 min. Its sensitivity is described as

$$-56 \text{ dBZ} + 20 \log_{10}(\text{height in kilometers}) \quad (1)$$

and is -36 dBZ at 10 km. A cloud retrieval algorithm (Wang and Sassen 2002; Mather et al. 2007) ingests data

TABLE 1. List of microphysical schemes tested. The column entitled “Hydrometeor classes” denotes the classifications of water for which the scheme predicts mixing ratios: Qc = cloud, Qr = rain, Qi = ice, Qs = snow, Qg = graupel, and Qh = hail. “Number concentration” indicates for which of the classes the scheme is two-moment.

Scheme	Reference	Hydrometeor classes	Number concentration
Goddard	Tao et al. (1989) Lang et al. (2007)	Qc, Qr, Qi, Qs, Qg	None
SBU-YLIN	Lin and Colle (2011) Lin et al. (2011)	Qc, Qr, Qi, Qs ^a	None
WDM6	Lim and Hong (2010)	Qc, Qr, Qi, Qs, Qg	CCN, ^b cloud, rain
Thompson	Thompson et al. (2008)	Qc, Qr, Qi, Qs, Qg	Ice, rain
Morrison	Morrison et al. (2009)	Qc, Qr, Qi, Qs, Qg	Rain, ice, snow, graupel ^c
Milbrandt	Milbrandt and Yau (2005)	Qc, Qr, Qi, Qs, Qg, Qh	All

^a Single class for “precipitating ice.”

^b Cloud condensation nuclei.

^c Two-moment for graupel is optional. The simulation shown in this paper does not use two-moment graupel. Another simulation (not shown) using two-moment graupel yields results that are similar to the simulation with one-moment graupel.

from the WACR and micropulse lidar at Niamey and combines them with merged sounding products (Trojan 2012) and microwave radiometer soundings (Morris 2006), which provide information on the vertical thermal and moisture structure of the troposphere. Almost all of the clouds observed in this study are detected by radar only. Reflectivity of the nonprecipitating anvil was corrected for gaseous attenuation by water vapor and oxygen using water vapor and temperature profiles from the merged sounding products as input for the Liebe (1985) radiative transfer model. The algorithm computes vertical distributions of rain, cloud ice, snow, and graupel in clouds passing over the AMF. Information on hydrometeor content from the retrieval serves as input for a radiative transfer code (Fu and Liou 1992), which is used to compute heating rates in observed anvil. Ice water content (IWC) is inferred from reflectivity using a binned reflectivity–temperature relationship (Protat et al. 2007):

$$\log_{10}(\text{IWC}) = 0.000457ZT + 0.0969Z - 0.0002T - 0.61, \quad (2)$$

where IWC is ice water content in grams cubic meter, Z is 95-GHz reflectivity in decibel units, and T is temperature in degrees Celsius. Ice particle size is calculated as a function of the ratio between ice water content and extinction (Fu 1996) for cloud elements for which both radar and lidar data are available. A fit to this ratio is calculated as a function of temperature over all the available radar/lidar data at Niamey and this climatological fit is used for periods when the lidar is attenuated and extinction is not available.

Figure 2 shows an example of observed W-band reflectivity and heating rates computed by the cloud retrieval and radiative transfer code for an MCS that passed

over the AMF on 19 July 2006. A leading anvil passes over the radar prior to 0500 UTC. The radar is strongly attenuated by heavy precipitation around 0600 UTC and is partially attenuated by lighter stratiform precipitation until about 1000 UTC. Beyond 1000 UTC, trailing anvil passes over the radar. Longwave radiation (Fig. 2c) heats the bottom of nonprecipitating anvil clouds, while radiation lost to space cools the tops of clouds, thus destabilizing them (Webster and Stephens 1980). However, during daytime, absorption of shortwave radiation leads to warming throughout the cloud (Fig. 2d). In the example shown, convergence of infrared and shortwave fluxes causes a net warming throughout most anvil clouds passing over the AMF between 1000 and 1400 UTC.

The profile of heating may vary significantly, however, depending on hydrometeor content within the anvil. For example, between 0400 and 0500 UTC, an anvil leading the MCS passed over the site. Reflectivity is primarily a function of IWC and hydrometeor size (Yuan et al. 2011; see their Fig. 4); however, other factors such as particle shape and density (Hong 2007) also have smaller-order effects on backscatter. Because of the strong relation between IWC and reflectivity, returns that vary greatly near the top and bottom of the leading anvil indicate that a sharp gradient in ice content is present near cloud top and base and more-uniform high ice amounts are present in a large region between (see Fig. 2a). As radiation encounters a gradient in IWC, unequal amounts are absorbed and reemitted. Therefore, longwave radiation heats or cools the cloud over a fairly small depth at the top and bottom of the anvil. In contrast, a smoother vertical gradient in reflectivity at the top of the trailing anvil does not imply a sharp gradient in ice content, and infrared cooling therefore occurs over a greater depth of the anvil while shortwave radiation penetrates deep into the cloud.

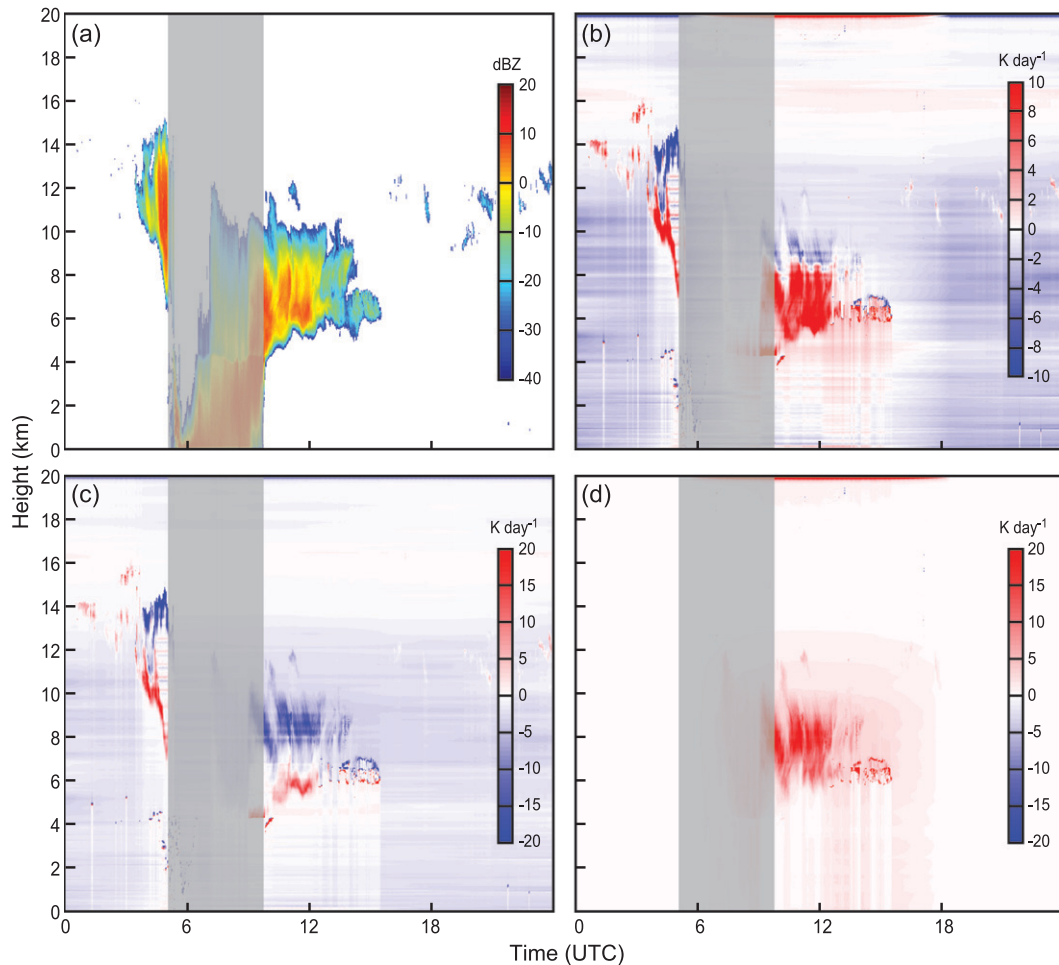


FIG. 2. (a) WACR reflectivity (dBZ) observed during the passage of an MCS over Niamey on 19 Jul 2006. (b) Heating rates (shortwave plus longwave; K day^{-1}) computed by a radiative transfer code after passing reflectivity data through a cloud retrieval. (c) As in (b), but for longwave radiation only. (d) As in (b), but for shortwave radiation only. Gray areas in each panel represent times during which WACR was partially attenuated by precipitation.

4. Statistical distribution of radar reflectivity in observed anvils

Fifteen MCSs passing over Niamey during 1 July–27 September 2006 were identified using methods of CH11. All MCSs consisted of leading convective lines with trailing stratiform regions, and all propagated westward at 13 m s^{-1} or greater. We classify anvil cloud as any nonprecipitating cloud that the WACR detects entirely above the 0°C level; any vertical profile that includes a reflectivity return below the 0°C level is considered precipitating. By using such a classification for anvil clouds, we avoid using radar data that have been attenuated by precipitating liquid water. We only classify as anvil the profiles contiguous with either other anvil profiles or the precipitating region of the MCS. We further subdivide anvil based on its thickness: Thin anvils

are those less than 2 km in depth, thick anvils are at least 6 km in depth, and all other anvils are medium. Our complete sample of anvil cloud is statistically small—field programs are designed for intensive observations of a few cases—nevertheless, previous studies have tested the robustness of the sample (CH11) and have shown that the statistics derived from it are consistent with a much larger sample of anvils detected by a polar-orbiting cloud radar (CH09).

Figure 3 illustrates several contoured frequency by altitude diagrams (CFADs; Yuter and Houze 1995) that represent the joint probability encompassing all 15 MCS cases of reflectivity occurring at various heights in each anvil subcategory. We normalize each CFAD by dividing the frequency in each height and reflectivity bin by the total number of all anvil profiles. Results are consistent with CH09 and Yuan et al. (2011). Thick

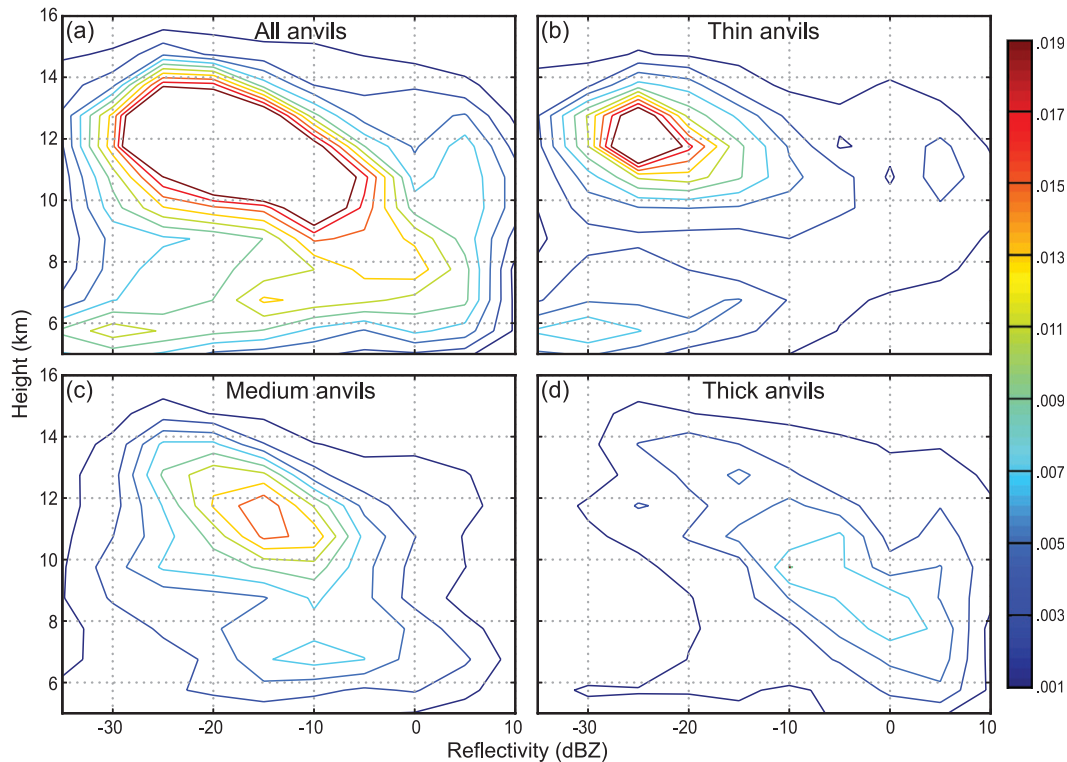


FIG. 3. CFAD for (a) all, (b) thin, (c) medium, and (d) thick anvils detected by WACR indicating the probability of detecting a reflectivity at a certain height. Contours range from 0.001 (dark blue) to 0.019 (dark red) with an interval of 0.002. Reflectivity and height are grouped by bins that are, respectively, 5 dBZ and 1 km in size. The contours show bin counts divided by total counts of all anvil profiles. Probability of detecting an anvil of given thickness at some height–reflectivity bin inside the innermost contour in (a) and (b) is greater than 1.9%.

anvils generally occur closest to the precipitating region and consist of smaller particles transported into the upper troposphere via deep convection and larger particles with larger fall speeds that are detected near cloud base. In the sample considered here, reflectivities of -10 to $+5$ dBZ are commonly observed in thick anvils at altitudes between 6 and 10 km. As anvils age and extend outward from the stratiform region, larger hydrometeors fall out, leaving longer-lived medium and thin anvils to consist of smaller particles at high altitudes (CH11). Medium anvils consist of some anvils that are barely deeper than thin anvils and others that are nearly 6 km thick. Therefore, as a whole, the modal distribution of medium anvils falls somewhere between thin and thick anvils in terms of both altitude and reflectivity: They are most likely to be detected between 10 and 12 km with reflectivities between -20 and -10 dBZ. Thin anvils in our sample most commonly occur between 12 and 13 km with reflectivities between -20 and -30 dBZ. The presence of some thin anvils between 5 and 7 km has been attributed to detrainment from shallow convection (Protat et al. 2010) associated with a mean tropical stable layer at that altitude (Johnson et al. 1999). Some thin anvils with

higher reflectivities, which mostly occur between 8 and 14 km, are associated with very young thin anvil extending from newly developing convective regions of MCSs.

Because the sensitivity of the WACR decreases in the upper troposphere, some very thin cirrus that extends from an anvil is not detected. For our study, this low sensitivity is not a major concern since we focus on the model's representation of anvil cloud, not thin, subvisible cirrus that remains after an MCS dissipates. Very few anvil clouds are detected by only lidar during the period examined, and these are excluded from our analysis. Therefore, the profiles of mean IWC shown in Fig. 4 are derived from the echo seen by WACR only. The shaded areas in Fig. 4 represent the span of the estimated root-mean-square error (rmse) predicted by Protat et al. (2007) as a function of IWC and serve as an error bound for the estimates of the mean IWC. For a value of IWC of 0.1 g m^{-3} , the rmse in the estimate corresponds to a fractional error of about $+50\%/-34\%$. We note that the profiles of median IWC (not shown) are generally nearly zero at all heights. The anvils that contain the largest amounts of ice heavily influence the mean IWC at each height for all classes of anvils. Therefore, profiles of mean

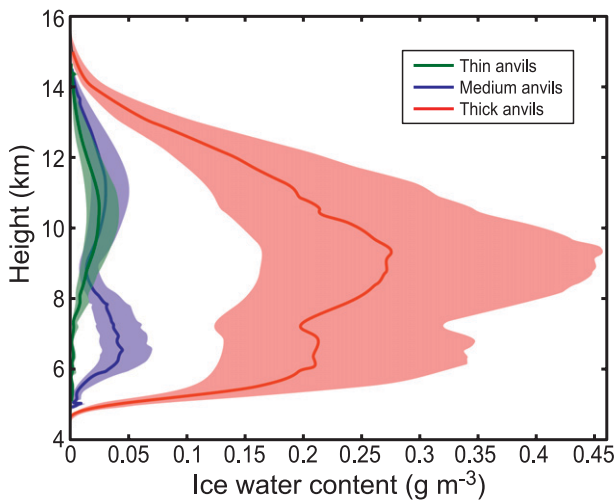


FIG. 4. Derived vertical profiles of ice water content (g m^{-3}) present in columns that contain anvil clouds detected by WACR. The solid lines represent the mean ice water content for thin (green), medium (blue), and thick (red) anvils. The shaded area spans the rmse of the cloud retrieval estimate of ice water content as listed in Protat et al. (2007).

IWC yield more information about the clouds with high IWC than the majority of clouds that have IWC that is lower than the mean. The largest mean values of IWC are a little more than 0.25 g m^{-3} and occur in thick anvils between 8 and 10 km, where we are most likely to detect reflectivities higher than -10 dBZ (see Fig. 3d). At most altitudes, IWC in medium and thin anvil is about an order of magnitude less than IWC in thick anvil at the same height. Since our sample of medium anvils is biased toward clouds only slightly deeper than 2 km, the mean IWC profile for medium anvils is similar to that for thin anvils at high altitudes; however, longer-lived thin anvils tend to contain less ice. A peak in mean IWC

of about 0.03 and 0.02 g m^{-3} for medium and thin anvils, respectively, occurs at around 11 km, and a secondary IWC maximum associated with lower-topped clouds occurs in medium anvils at about 7 km.

The radiative heating profiles shown in Fig. 5 characterize heating that occurs inside anvils. To highlight both infrared heating near cloud base and cooling at cloud top, we have normalized the height coordinate by cloud thickness. The base of the cloud always occurs at a normalized height (NH) of 0, and cloud top always occurs at $\text{NH} = 1$. Note that many of the MCSs that pass over Niamey—including all three simulated in this study—approach overnight. In such systems, the leading anvil experiences no solar radiative fluxes. However, trailing anvil often lingers throughout the following morning and afternoon, and solar fluxes become important to consider after daybreak. Since the mean longwave heating is heavily influenced by particularly large values of heating and cooling near the bases and tops of anvils, we have chosen to depict the median longwave heating rates in Fig. 5. However, the intensity of incident solar radiation varies with time of day and is zero at night, and median solar (shortwave) heating rates are nearly zero at all heights. Therefore, shortwave heating profiles in Fig. 5 are averaged over the entire sample so that our resulting profiles are representative of the composite mean heating in all daytime and nighttime anvils. Many assumptions about ice habit must be made in the cloud retrieval to estimate properties such as IWC and particle size. Such assumptions yield both positive and negative errors for the properties estimated, which impact our calculations of radiative transfer. In addition, spatial and temporal variability naturally occur in anvil structure. To address both uncertainties in our estimates of in-cloud heating, the gray shaded area in Fig. 5 represents the middle 80%

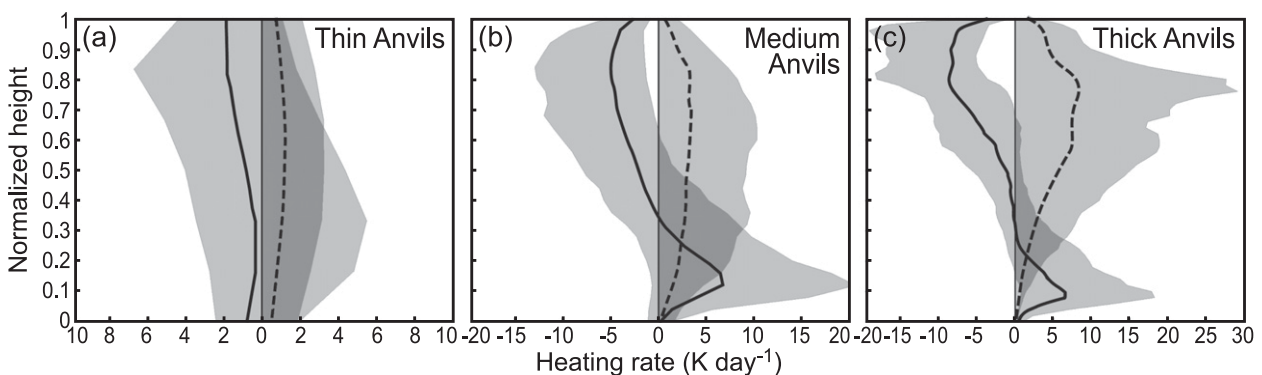


FIG. 5. In-cloud heating rates (K day^{-1}) computed by a radiative transfer code for (a) thin, (b) medium, and (c) thick anvil clouds detected by WACR. Height is normalized, so that the cloud base occurs at 0, and the cloud top occurs at 1. Solid lines depict median longwave (LW) heating rates, and dashed lines represent mean shortwave (SW) heating rates. The shaded area contains the inner 80% of the distribution of heating rates observed at each normalized height. The thin vertical black line represents zero heating.

of heating rates derived for anvil clouds at each normalized height and for each class of anvil.

Longwave cooling is generally largest near the tops of thick anvils, and cooling at rates of about 10 K day^{-1} commonly occurs near cloud top. Cooling of as much as 20 K day^{-1} is observed within the middle 80% of thin anvil heating. In Fig. 4, we notice that with decreasing altitude in a thick anvil profile from 16 to 12 km, IWC rapidly increases. Therefore, the majority of longwave cooling occurs where a sharp gradient in IWC exists near cloud top. Below the region of strongest cooling, only weak cooling occurs in thick anvils at NHs between 0.3 and 0.7. Warming near the bases of thick anvils is comparable to that of medium anvils, and maximum heating rates near the bases of either are typically as high as $15\text{--}20 \text{ K day}^{-1}$ and occur at an $\text{NH} = 0.1\text{--}0.2$. Medium anvils experience cooling near cloud top at rates of $2\text{--}13 \text{ K day}^{-1}$, with a median of about 5 K day^{-1} at $\text{NH} = 0.8$. Thin anvils show no distinct pattern of warming at cloud base and cooling aloft. The middle 80% of heating rates for thin anvils spans both cooling and heating at all NHs, although the distribution of heating rates is skewed toward cooling near cloud top and heating near cloud base. They generally experience radiative fluxes of lower magnitude throughout the cloud; heating or cooling on the order of $5\text{--}7 \text{ K day}^{-1}$ is typical in thin anvils. Medium and thick anvils exhibit a level of zero longwave heating (hereafter LZLH) somewhere between $\text{NH} = 0.2$ and $\text{NH} = 0.7$, and their median LZLH is near $\text{NH} = 0.3$. Shortwave heating reaches a maximum slightly below cloud top near an NH of 0.8 for medium and thick anvils and decreases gradually toward cloud base, presumably as much of the radiation is absorbed and reemitted as longwave radiation. Thick anvils exhibit stronger shortwave heating (as much as 25 K day^{-1}) than thin anvils ($\sim 1\text{--}2 \text{ K day}^{-1}$), which have more uniform shortwave heating throughout their depth.

We next compare the data depicted in Figs. 3–5 with the results from model simulations carried out with different microphysical schemes.

5. Comparison of model and observed anvil reflectivity statistics

While the model does not exactly replicate the structure of each MCS, it does produce MCSs of comparable size that contain a convective squall line followed by a precipitating stratiform region and anvil. Environmental temperature data from radiosondes compare well with the modeled temperature profiles, and both indicate a tropopause height of about 16–17 km for the 19 July and 11 August cases and 15–16 km for the 8 September case. Again, we only consider for our

analysis nonprecipitating anvil cloud above the freezing level. As such, anvils consist of hydrometeors classified as either snow or ice by each microphysical scheme. To directly compare model results to CFADs produced using ARM data, we convert IWC in the model to a simulated WACR reflectivity using the same relationship among IWC, reflectivity, and temperature for tropical clouds as we used in the cloud retrieval. While the $\text{IWC}\text{--}Z\text{--}T$ relationship in (1) is fit to the linear mean IWC using 5-dB reflectivity and 5°C bins, we do not group model output by any temperature or IWC intervals. The relationship between reflectivity and ice water content depends largely upon the ice habit as described by Kulie et al. (2010). However, since Protat et al. (2007) use multiple in situ datasets to derive their $\text{IWC}\text{--}Z\text{--}T$ relationship, the uncertainty in their relationship is at least partially representative of the various ice habits that are likely observed in situ. To take into account different ice habits, a better approach should be used in the future to simulate reflectivity using modeled IWC. In addition to mixing ratios for each hydrometeor class, predictions of their number concentrations or assumed particle size distributions could also be used to simulate reflectivity. The density and shape of hydrometeors also varies between schemes. Radar simulators that use such information from microphysical schemes remain under development (Masunaga et al. 2010). Although not shown, we have also made the comparisons in terms of IWC by comparing IWC derived from radar observations to modeled IWC. The distributions of IWC with height vary little from the distributions of reflectivity with height. We have chosen to present our results in terms of reflectivity because we may compare our uncertain model results against a direct measurement rather than an uncertain quantity derived from that measurement. Our current method of simulating reflectivity still provides a stringent test for the model that can be applied to one-moment or two-moment schemes because it requires each scheme to correctly model IWC in order to reproduce realistic reflectivity distributions.

Table 2 gives the percentage of occurrence of the three anvil classes for simulated and observed clouds. Relative frequencies of observed anvil cloud closely match observations from Niamey as seen in Protat et al. (2010; see their Fig. 5). They found that the majority of clouds at Niamey have thicknesses less than 2 km and that few clouds are observed with thicknesses greater than 5 km. Figures 6–11 present CFADs [(d)–(g) of each figure] for each of the six microphysical schemes tested with mean vertical profiles of ice and snow mixing ratios [(a)–(c) of each figure] for each of the anvil classes. Figure 12 represents mean IWC vertical profiles (ice plus snow mixing ratios multiplied by air density) for

TABLE 2. Relative frequency of occurrence for thin, medium, and thick anvils observed by WACR and simulated in the WRF by each microphysical scheme.

Scheme	Thin anvils	Medium anvils	Thick anvils
ARM	0.66	0.26	0.08
Goddard	0.61	0.30	0.09
SBU-YLIN	0.43	0.35	0.21
WDM6	0.68	0.26	0.06
Thompson	0.41	0.38	0.21
Morrison	0.40	0.38	0.22
Milbrandt	0.43	0.41	0.17

each scheme separated by anvil classification. Graupel is treated as a large particle with a higher fall velocity than ice or snow; therefore, almost all of it precipitates out before reaching the nonprecipitating anvil, and we do not include it in our computations of IWC. Inclusion of graupel in our analysis (not shown) does not affect the results. Each CFAD and all subsequent figures represent a composite of anvil cloud from all three cases simulated.

The Goddard microphysical scheme (Fig. 6) produces realistic relative amounts of all types of anvils. As shown in Table 2, it is one of two microphysical schemes evaluated in which about two-thirds of the total simulated anvil cloud is thin, in good agreement with observations. The CFAD for thin anvils indicates that they occur most often around 12 km; however, their modal simulated reflectivity is about 5 dBZ too low. Since reflectivity is largely a function of hydrometeor size and amount, and the Goddard scheme only predicts hydrometeor mixing ratios, we deduce that the model transports too little ice to its thin anvils. The vertical profiles of IWC for modeled anvil clouds confirm that, compared to IWC derived from observations (grayscale in Fig. 12) the Goddard scheme produces realistic amounts of ice in thick anvils (Fig. 12c), particularly between 6 and 10 km. Estimates of IWC in medium anvils (Fig. 12b) are close to the lower error bar depicted by the grayscale region. The scheme clearly underestimates the amount of ice present in thin anvil profiles (Fig. 12a). Interestingly, the Goddard scheme also appears to effectively reproduce some of the thin

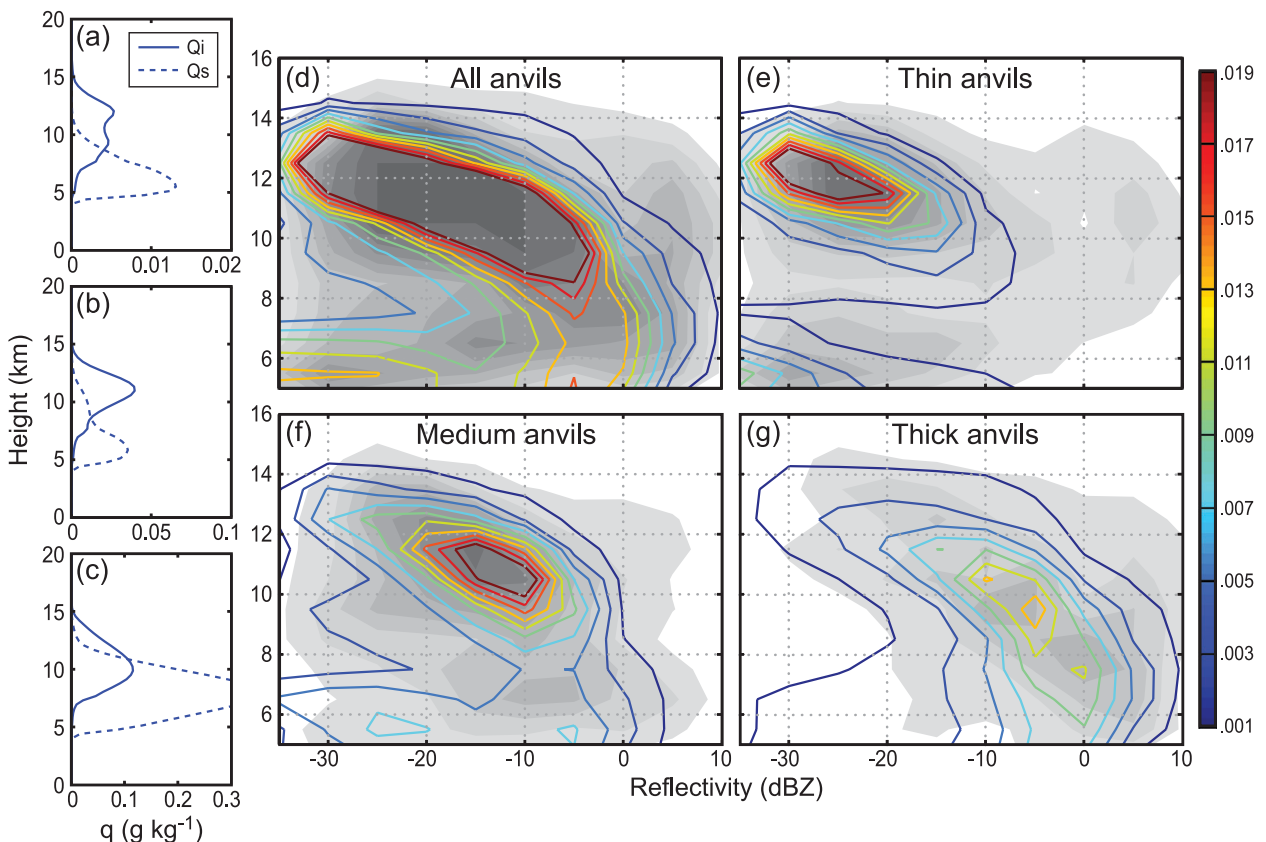


FIG. 6. Mean vertical profiles of mixing ratios (g kg^{-1}) of ice (solid) and snow (dashed) for (a) thin, (b) medium, and (c) thick anvils generated by the WRF using Goddard microphysics. Note the difference in scale on the abscissa of each plot. (d)–(g) CFADs for anvil clouds generated by the WRF using Goddard microphysics overlaid on CFADs for ARM anvil clouds (grayscale). Colored contour interval is as in Fig. 2.

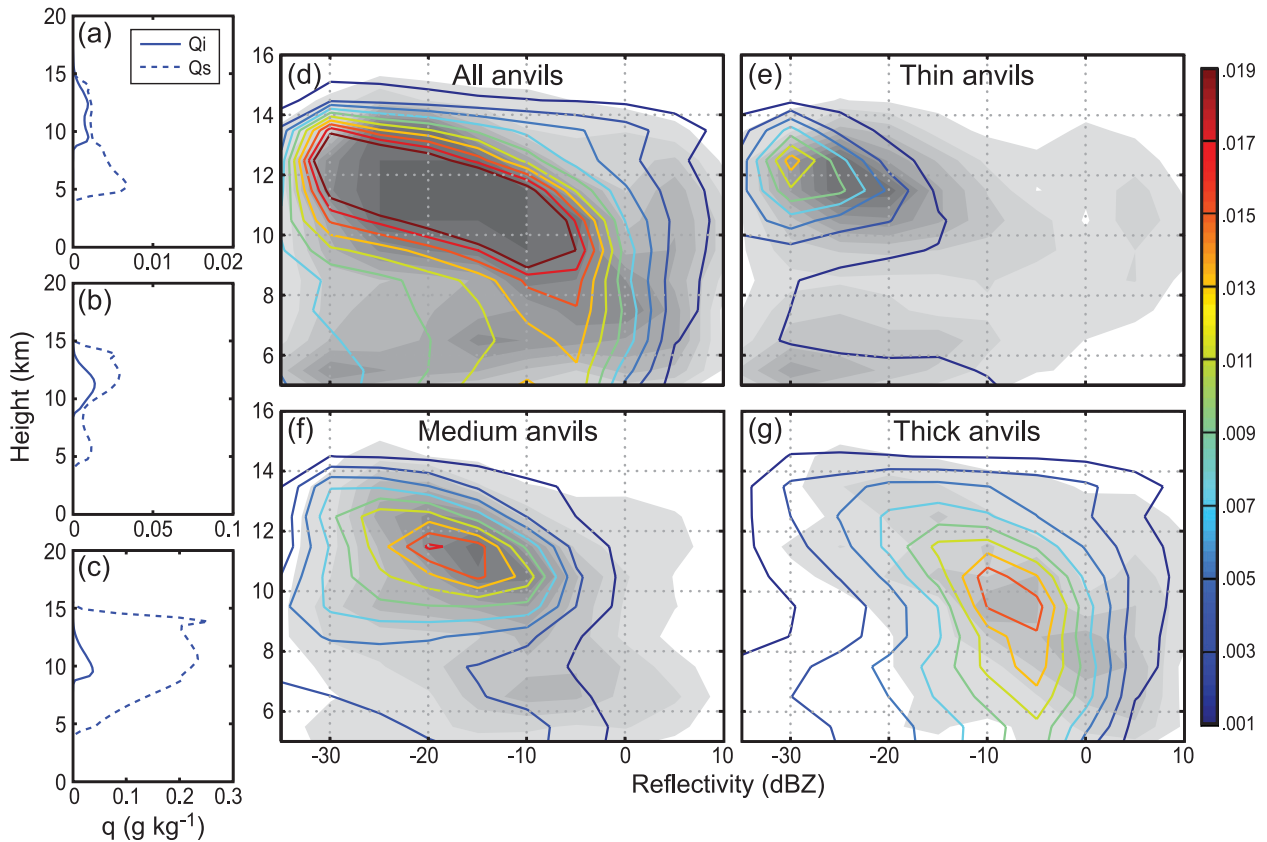


FIG. 7. As in Fig. 6, but for SBU-YLIN microphysics.

cloudiness detrained from shallow convection around 6–7 km. Figure 6d shows that about a 0.01 probability exists for finding a thin anvil located near 6 km with a reflectivity of -30 dBZ. Figure 6a suggests that such shallow convection is composed almost entirely of snow but that thin anvil that occurs above 10 km is composed of only smaller ice particles. The scheme does well in its representation of medium anvils and their reflectivities; however, they occur too frequently near their modal distribution, which is centered at 11 km and -15 dBZ. Similar to thin anvils, higher medium anvils consist of mostly ice while those below 9 km contain mostly snow. The shape of the CFAD for thick anvils closely resembles that of observed anvils. Simulated thick anvil is modally distributed between -10 and 0 dBZ and from 6 to 10 km in altitude. We expect higher reflectivities at such altitudes since simulated thick anvil consists of a high amount of large snow crystals near cloud base. However, the yellow and orange contours in Fig. 6g suggest that the model may not form enough variety of thick anvil. For example, while the scheme produces more thick anvil in its modal distribution than what we observe, it underrepresents highly reflective thick anvil occurring at high altitude.

Since the SBU-YLIN scheme (Fig. 7) is similar to the Goddard scheme, we might expect that they yield similar results. However, SBU-YLIN produces too much medium and thick anvil. Thin anvil does not occur frequently enough, and when it does occur, it often has a reflectivity of about -30 dBZ, although the altitude of the cloud is realistic. Thin anvil with higher reflectivity is not simulated. Although the scheme produces too much medium anvil, it does well at representing the distribution of reflectivity found in observed medium anvil. The simulated medium anvil occurs frequently near 11 km with reflectivity between -25 and -15 dBZ. The range of thick anvil reflectivities across various altitudes is also well represented; however, the scheme produces too much thick anvil near 9–10 km with a reflectivity between -10 and 0 dBZ. In fact, the modal distribution of thick anvil using SBU-YLIN occurs between -10 and 0 dBZ from near the 0°C level to beyond 11 km. When compared to frozen water profiles computed for Goddard thick anvils, more snow and less ice is produced by SBU-YLIN above 10 km, and less snow is present below 10 km. We propose that too much riming occurs in SBU-YLIN, thereby exhausting ice particles needed to maintain thin anvils. Since the larger aggregates have greater

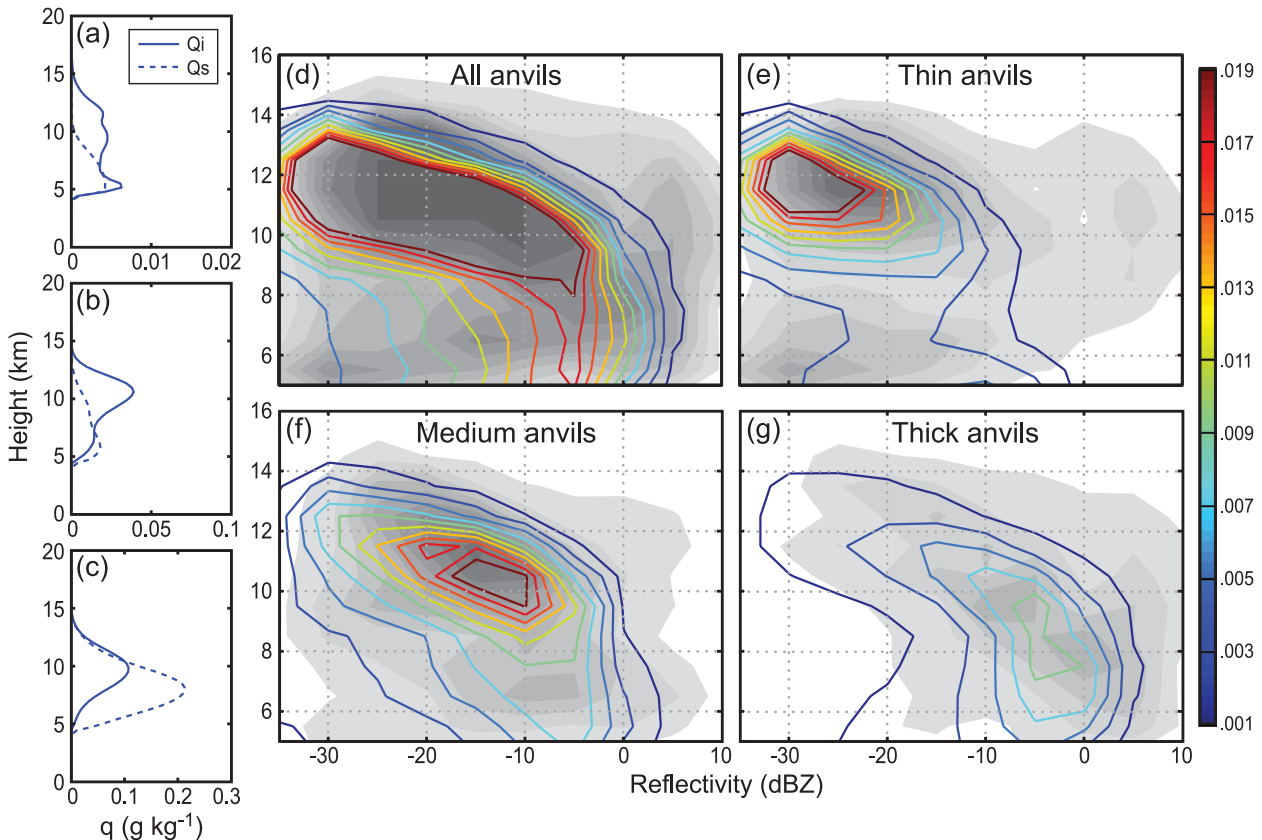


FIG. 8. As in Fig. 6, but for WDM6 microphysics.

fall velocities, hydrometeor distribution extends closer to the 0°C level in a greater number of clouds. However, not enough snow is present near cloud base for anvils to be highly reflective. SBU-YLIN produces the highest relative amount of thick anvil of any of the schemes tested: About 20% of all anvils simulated by the scheme are thick. Additionally, despite having high snow mixing ratios—particularly in thick anvil—very little cloud ice is present in any anvil class, and as a result, total IWC in all anvils is too low (Fig. 12).

The WDM6 scheme (Fig. 8) also produces realistic anvil cloud of all types. Modeled anvils occur at approximately the correct frequency: About two-thirds of anvils are thin, and roughly one-quarter are medium. Thin anvils occur most often at about 12 km, and their reflectivities most frequently range from -35 to -25 dBZ—about 5 dBZ less than thin anvils observed by WACR. The distribution of reflectivity among medium anvils is well represented and the modal distribution extends correctly toward higher reflectivity at lower heights; however, cloud is present about 1 km lower than observed medium anvil. The modal distribution of thick anvils is mostly well simulated: Such anvils occur most often between 6 and 10 km at reflectivities of -10 – 0 dBZ, although

the scheme appears to struggle with the most highly reflective clouds near 6–8 km. The scheme does not yield many high reflectivities near the tops of high-reaching thick anvil. Similar to the Goddard scheme, high and thin anvils are composed of mainly cloud ice. The tops of medium and thick anvils contain predominantly cloud ice, while the bases of thick anvils and some deeper medium anvils contain mostly snow. The mixing ratios of cloud ice and snow are comparable to those generated by the Goddard scheme for all anvils, except that WDM6 produces slightly more snow between 5 and 10 km. IWC in thick anvils in the WDM6 is slightly less than in the Goddard scheme, but IWC in thin and medium anvils is comparable to that seen in the Goddard scheme.

The Thompson scheme (Fig. 9) also produces excessive medium and thick anvil. Because of the efficient conversion of cloud ice to snow, all simulated anvils contain essentially no cloud ice. IWC profiles of all anvil clouds are reasonable; however, too much water appears to be stored in thick anvils. IWC near the tops of thin anvils is too small. IWC in medium anvils is comparable to observations but about 50% less than Goddard IWC, and IWC in thick anvils is mostly within the error bounds depicted in Fig. 12c. Thin anvils in the

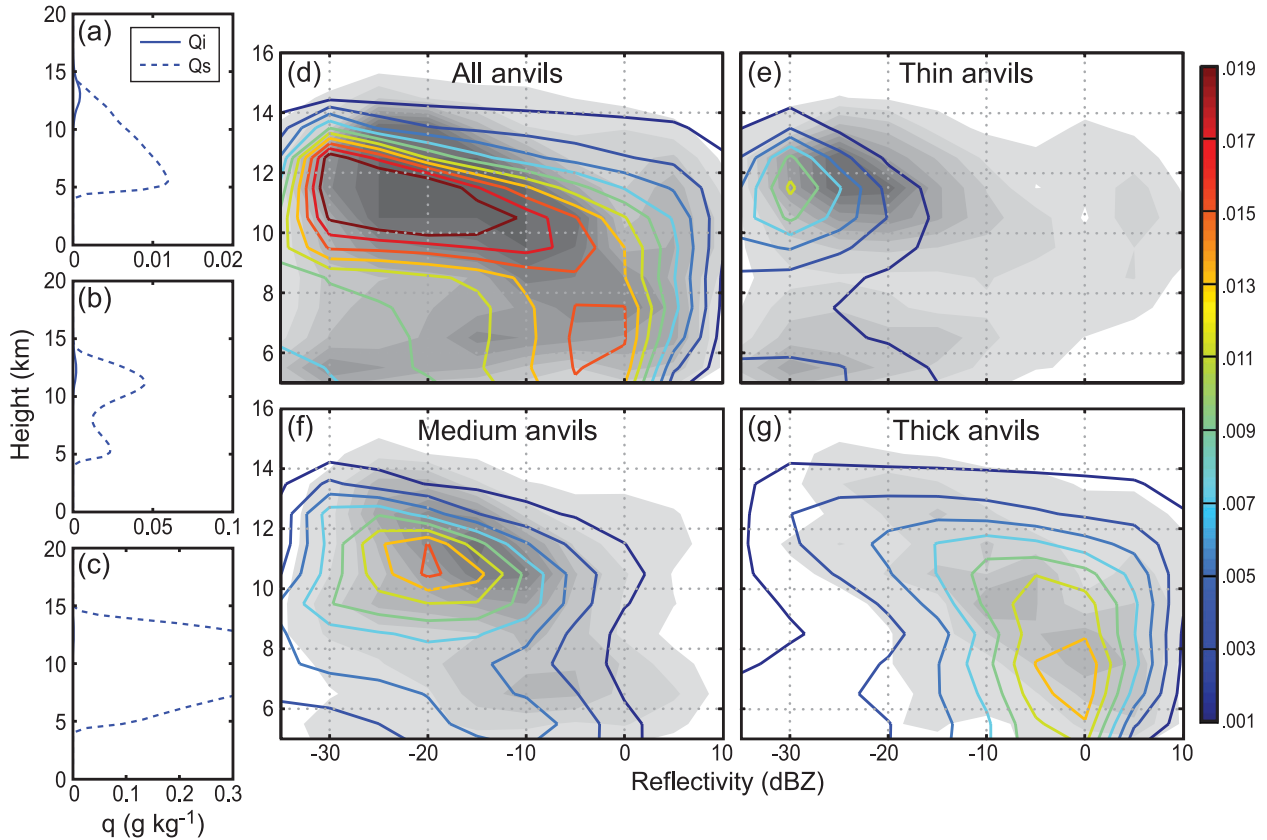


FIG. 9. As in Fig. 6, but for Thompson microphysics.

Thompson scheme occur too infrequently, only slightly lower than those observed, and with reflectivities of about -30 dBZ. No thin anvils have reflectivities higher than -15 dBZ. Medium anvils occur most frequently around 11 km in the model, and the mode in reflectivity occurs near -20 dBZ. The amount of water present in thick anvils is much greater than that seen in the other schemes and, as a result, simulated reflectivities greater than 0 dBZ occur too frequently at all heights. Nonetheless, most thick anvils are simulated between 5 and 9 km with a reflectivity near or slightly less than 0 dBZ. As with the SBU-YLIN scheme, the mode in reflectivity distribution occurs between -10 and 0 dBZ at various heights, and the modal distribution does not extend toward higher reflectivities at lower altitude.

While the Morrison scheme (Fig. 10) also generates too much medium and thick anvil, clouds occur at higher altitudes than when we use any other parameterization. Thin anvils occur most often above 12 km with reflectivities slightly above -30 dBZ. Thin anvils with reflectivity higher than -15 dBZ are completely unrepresented. Simulation of medium anvils reveals that the model frequently reproduces high cloud between 11 and 14 km with reflectivities between -20 and -10 dBZ;

however, it does not develop more optically thick medium anvil observed between 6 and 8 km. Thick anvils occur most often between 9 and 12 km, and those clouds have simulated reflectivities between -15 and -10 dBZ. Mean profiles of cloud ice or snow suggest far less water is present in anvil than in better performing schemes, and Fig. 12 further indicates low IWC in its anvil regardless of thickness. Although mean IWC profiles indicate that too little ice is present, the total amount of water transported into the anvil may be reasonable. To prevent formation of large numbers of ice crystals via homogeneous freezing, the Morrison scheme imposes a maximum ice concentration of $10\ cm^{-3}$, which is about one order of magnitude higher than in the Thompson scheme (G. Thompson and H. Morrison 2011, personal communication). Higher potential ice crystal concentrations in the Morrison scheme allow its particle size distribution to include more small ice crystals with lower sedimentation velocities. Ice then expands over a larger spatial area before falling out. As such, water stored in anvils may not be as concentrated as in other schemes.

The Milbrandt scheme (Fig. 11) generates too much medium and thick anvil. Its distribution of reflectivity also has a low bias consistent with low amounts of ice

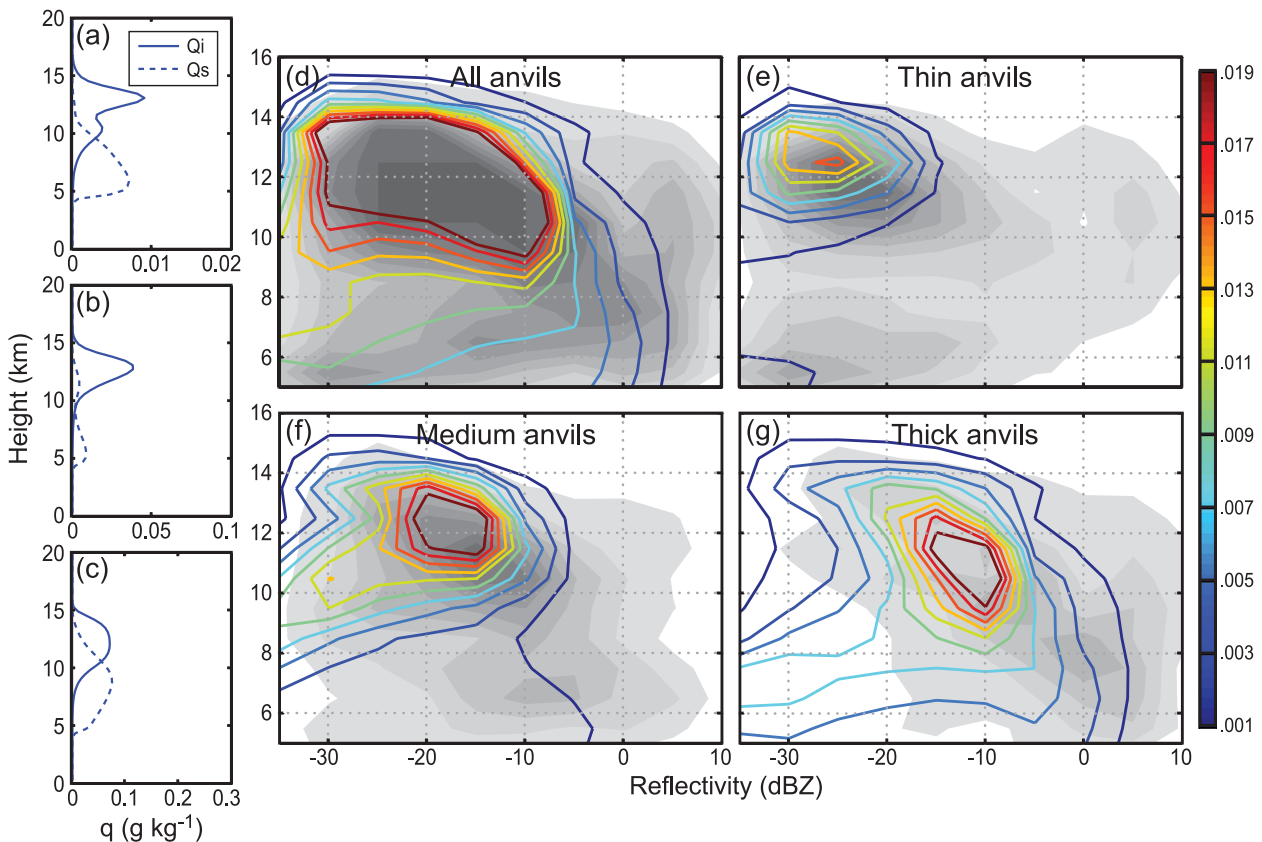


FIG. 10. As in Fig. 6, but for Morrison microphysics.

present in the simulated clouds (Fig. 12). Figures 11a–c show that mixing ratios of snow in all anvil classes are much lower than those generated by the better performing Goddard or WDM6 schemes, especially for thicker anvils. Thin anvils occur most frequently near 11 km with a reflectivity of about -30 dBZ. Medium anvils are placed slightly lower than those observed, and the modal reflectivity is only slightly lower than the ARM anvils. The range of simulated reflectivity in medium anvils is well treated; however, the modal distribution extends toward more optically thin clouds at lower levels, unlike clouds seen in observations. Thick anvils are mostly constrained to between 8 and 12 km, and although the wide range of simulated reflectivity at various heights is realistic, IWC and reflectivity near the bottoms of the thick anvils are much less than those derived from observations. In fact, the Milbrandt scheme produces very little anvil in any class with a reflectivity higher than 0 dBZ.

Although thin anvils simulated by all schemes contain too little cloud ice, the Goddard and WDM6 schemes, which both use ice microphysics based on L83 and RH84 with minimal adjustments, appear to show generally exceptional agreement with observations of tropical anvils

over West Africa. Meanwhile, the other schemes generally show a wide range of potential reflectivities in medium and thick anvils at various heights consistent with anvils observed by radar. Most also show a maximum in ice content between 8 and 10 km in thick anvils as well as two maxima in ice content associated with medium anvils at about 6 and 11 km. However, they incorrectly reproduce the reflectivity distribution across various heights. Such schemes suffer most clearly from two problems: 1) not enough thin anvil being produced relative to thick anvil, and 2) ice water content being too low in all classes of anvil.

Many medium and thin anvils are simply remaining upper portions of formerly thick anvils that have since precipitated out larger particles near their bases as they move farther from the convective region from which they formed. Since IWC in modeled thick anvils of some of the schemes matches or exceeds that in those observed, we hypothesize that production of cloud ice within upper portions of the anvil is not sufficiently parameterized, the fallout rate of cloud ice is incorrect, or not enough water is transported into the upper anvil. Further investigation into the schemes will be necessary to determine how to improve their representations of

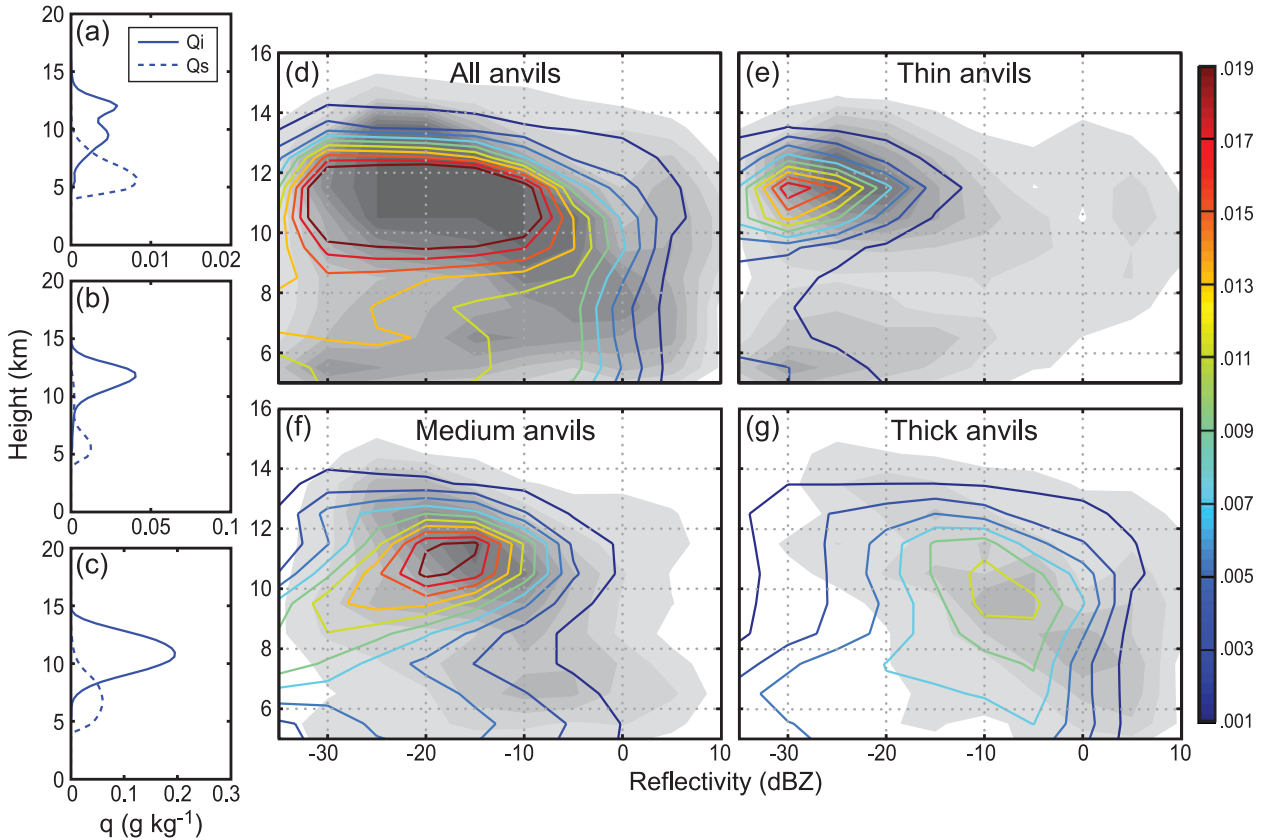


FIG. 11. As in Fig. 6, but for Milbrandt microphysics.

precipitating regions, anvil clouds, and water transport between precipitating and nonprecipitating portions of tropical MCSs.

6. Anvil-top heights

The height of the tops of anvil clouds is most influenced by the depth of convective cores, which in turn is affected by how the dynamics of the model respond to large-scale environmental conditions. The heights of longer-lived anvils may also be influenced by hydrometeors present in the anvil and how quickly those particles sediment out. After we simulate WACR reflectivity using (2), anvil top in our simulations is defined as the altitude of the highest grid point at which the simulated reflectivity exceeds the sensitivity of WACR, given by (1), in a model column. Using the sensitivity of the WACR as a cutoff for anvil classification allows us to directly compare simulated anvil heights to those observed by the cloud radar.

Figure 13 depicts probability density functions (PDFs) of cloud-top height in the ARM observations as well as anvils simulated in WRF using each microphysical scheme. The anvil clouds observed by cloud radar for

15 MCS cases show a bimodal distribution in thick anvil-top height, which is indicative of the variation in depth of convective cores from case to case. Thick anvils extend above 13 km in more than two-thirds of those sampled. Medium anvils most frequently have tops near 14 km, and longer-lived thin anvils most often have lower tops near 13 km. The model simulations produce anvils that usually reach as high as 13–15 km and are broadly consistent with cloud-top heights derived from the radar dataset. We do not detect the bimodal distribution of thick anvil-top heights in the model simulations because the three cases that we choose to simulate were all observed to have convection deeper than 13 km.

The PDFs of simulated thin anvil-top heights are mostly similar to those determined by cloud radar. However, the following discrepancies are evident. Medium and thick anvil tops occur too low in the Goddard, Thompson, and WDM6 schemes. All anvils produced by the Milbrandt scheme are systematically too low (peaks in the PDF for thick, medium, and thin anvils occur respectively at 13, 13, and 12 km). The Morrison scheme systematically produces anvils that extend too high: the peak in the PDF for each class of anvil occurs at 14 km, and very few cloud tops are seen below 12 km. The

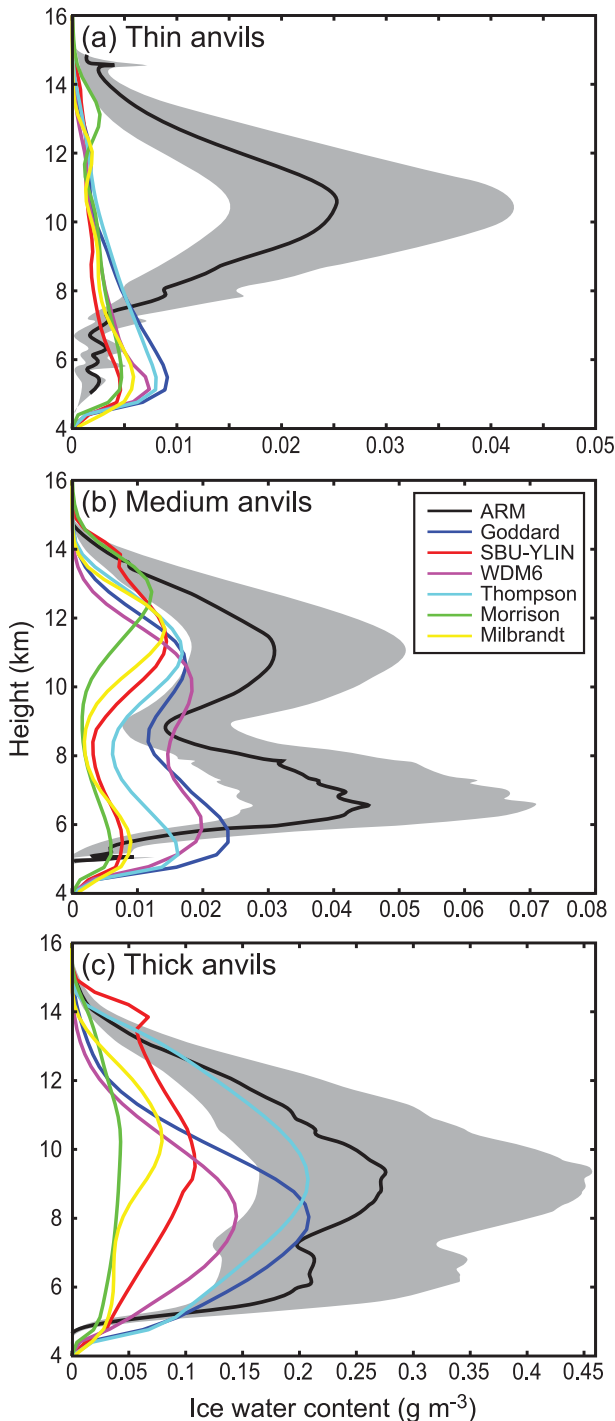


FIG. 12. Vertical profiles of mean ice water content for columns that contain (a) thin, (b) medium, and (c) thick anvil clouds observed by WACR (black) and modeled in the WRF using the Goddard (blue), SBU-YLIN (red), WDM6 (magenta), Thompson (cyan), Morrison (green), and Milbrandt (yellow) schemes. The gray shaded area for each class of anvils is the same as the corresponding shaded area in Fig. 4.

distribution of cloud top in SBU-YLIN is mostly realistic; however, it produces too much anvil of each class near 14 km.

7. Radiative heating profiles

Each microphysical scheme produces different amounts of cloud ice and snow crystals in anvil clouds. Furthermore, the evolution of IWC in anvils is treated differently by each scheme. The uncertainty involved in parameterizing transport of water to the anvils means that clouds produced by each scheme will affect radiative heating in the troposphere somewhat differently. Using output from RRTM in WRF, we have generated heating profiles for each microphysical scheme and each classification of anvil in order to investigate the range in magnitude and height over which radiative heating fluxes most likely occur inside of anvil clouds. As described in sections 2 and 3, treatment of cloud ice in RRTM is very similar to that in the radiative transfer code used by the cloud retrieval. Therefore, the heating rates simulated by the model can be directly compared to those derived from radar observations.

Figure 14 shows in-cloud median longwave heating profiles normalized by anvil thickness for thin, medium, and thick anvils. Since timing of MCS formation and passage in the model differs from that in the observations by 4–6 h, we do not include shortwave heating profiles. Variation of the solar incidence angle over that period would change significantly enough to prevent directly comparing modeled shortwave heating to observed heating. Thin anvils not fully resolved by the model—those entirely contained within one grid box—are not included in Fig. 14a since we normalize height by anvil thickness. Exclusion of such anvils does not greatly change the relative frequency of each anvil type.

Median longwave heating and cooling is well represented in thin anvils for most schemes. Only the Morrison scheme has median heating rates that ever fall outside of the middle 80% of heating in observed anvils. Thin anvils in the Morrison scheme typically experience warming throughout the depth of the cloud, which is contrary to that seen in observations or any other scheme. WDM6 shows more pronounced heating near cloud base and cooling aloft—with rates on the order of $2\text{--}4\text{ K day}^{-1}$. Since the median ice water content in observed thin anvils is nearly zero, and the model underrepresents ice in anvils, we should expect that median heating rates in the model would closely parallel those observed. Mean heating rate profiles (not shown) are more descriptive of the clouds with the strongest heating and cooling and, for thin anvils especially, illustrate more variability from scheme to scheme.

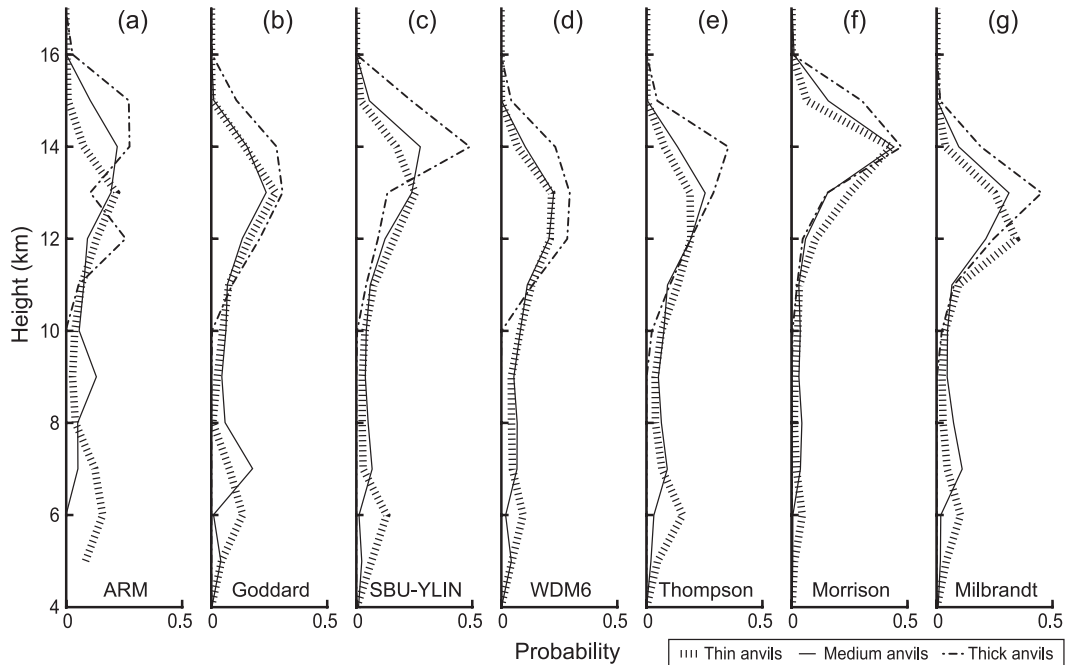


FIG. 13. Probability density functions for the height at which an anvil cloud top will be detected for anvils (a) observed by WACR, or produced in the WRF using (b) Goddard, (c) SBU-YLIN, (d) WDM6, (e) Thompson, (f) Morrison, and (g) Milbrandt microphysics.

The profile of simulated heating rates in medium anvil varies more by scheme. Cooling occurs at the top of clouds, and warming occurs near the base of the cloud regardless of the scheme used. The Goddard, Thompson, and SBU-YLIN schemes most closely represent the magnitude of longwave cooling near cloud top and include maximum cooling of about 10 K day^{-1} near $\text{NH} = 0.95$. Their LZLHs occur at $\text{NH} \sim 0.4$ (Goddard) and $\text{NH} \sim 0.6$ (Thompson and SBU-YLIN), which is higher than the observed median LZLH of $\text{NH} = 0.3$ but still within the middle 80% of observed heating rates. Their maxima in heating of $2\text{--}5 \text{ K day}^{-1}$ occurs at $\text{NH} \sim 0.3$, compared to a maximum at about $\text{NH} = 0.1$ in observed medium anvils. Median cooling in the WDM6 at $\text{NH} = 0.9$ is about 15 K day^{-1} , and the LZLH in WDM6 is near $\text{NH} = 0.4$. Maximum heating occurs near $\text{NH} = 0.2$ but only has a magnitude of about 2 K day^{-1} . Again, the three schemes that produce the least amount of cloud ice and snow in lower portions of the anvil (SBU-YLIN, Morrison, and Milbrandt; review Fig. 12b) yield anvils throughout which mostly longwave heating occurs. Heating extends too high into the anvil in both the Morrison and Milbrandt schemes, which both have an LZLH near $\text{NH} = 0.7$, and the magnitude of maximum heating in the Morrison scheme is near 10 K day^{-1} at $\text{NH} = 0.4\text{--}0.5$.

Most of the simulations very effectively replicate the location and magnitude of longwave cooling near the

tops of thick anvils. Although the Milbrandt scheme depicts median cooling in excess of 20 K day^{-1} near cloud top, all other schemes produce cooling at rates of $14\text{--}16 \text{ K day}^{-1}$. None of the schemes yield anvils that have sufficient warming near their bases. Nonprecipitating liquid water beneath modeled thick anvil that is not present in observations may absorb and reemit longwave radiation at a temperature lower than the surface temperature. Therefore, longwave heating is distributed throughout the area beneath the cloud, and the heating maximum near the base of the frozen cloud is not realized. Additionally, the LZLH for each scheme occurs at $\text{NH} = 0.4\text{--}0.7$, and median cooling goes to essentially zero for all schemes at $\text{NH} = 0.7$. In the middle of thick anvils, where we observe cooling rates below 5 K day^{-1} , we simulate either slight warming or cooling at rates less than 2 K day^{-1} . Only the Milbrandt and Morrison schemes—which both produce thick anvils containing small amounts of water—show a distinctive peak in warming at a magnitude of $1\text{--}2 \text{ K day}^{-1}$, but it occurs at an $\text{NH} \sim 0.4$.

8. Conclusions

Using a high-resolution weather forecasting model (WRF version 3.3), we have simulated three mesoscale convective systems observed by instrumentation at Niamey, Niger, during the summer of 2006. We have

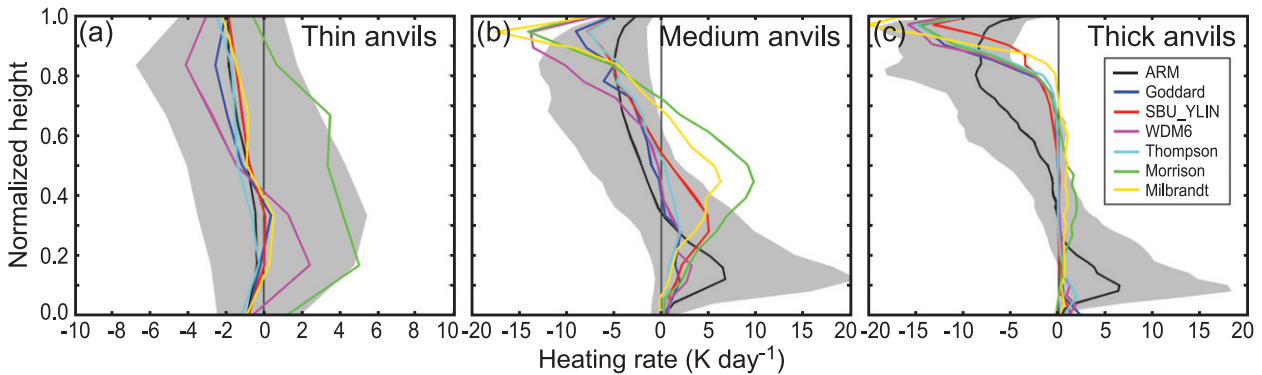


FIG. 14. In-cloud median radiative heating rates scaled by normalized height for (a) thin, (b) medium, and (c) thick anvils observed by WACR (black) and produced in the WRF simulations using Goddard (blue), SBU-YLIN (red), WDM6 (magenta), Thompson (cyan), Morrison (green), and Milbrandt (yellow) microphysics. The thin black line in each represents zero heating.

simulated each case using six microphysical schemes that have been recently developed and/or incorporated into the WRF. We use observations obtained by W-band cloud radar as input for a cloud retrieval, which allows us to estimate in-cloud heating rates of continental tropical anvil clouds. The radar reflectivity observations and radiative heating rates inferred from the observations serve as a verification dataset for model output.

Based on the results of our simulations, we have reached the following conclusions:

- 1) In the most realistic simulations, thin anvils, as well as the tops of medium and thick anvils, consist of small ice particles, while larger precipitating hydrometeors are more numerous near the bases of medium to thick anvils.
- 2) The typical longwave radiative heating profile in anvils of all thicknesses consists of strong cooling at cloud top and strong warming in a thin layer near cloud base. The profile is sensitive to the vertical gradient of ice water content at the upper and lower boundaries.
- 3) The Goddard and WDM6 schemes, which use a single-moment approach for ice-phase hydrometeors, produce the most realistic anvils. Among the two-moment ice schemes, the Thompson scheme seems to most closely simulate the profiles of ice content and reflectivities seen in observed anvils. Other schemes have problems producing the correct amount of thin anvil, and their anvils either contain too little snow and ice or too much snow and not enough smaller ice particles. All schemes produce too little cloud ice in high-altitude thin anvils. Potential problems with ice microphysics in anvils or water transport throughout an MCS must be investigated in future studies.
- 4) Heights of cloud tops for each anvil class vary depending on the microphysical scheme used but are generally near the level of observed cloud tops, suggesting that dynamics driving the depth of convection in the model are realistic.
- 5) In simulated thin anvils, median longwave cooling is properly represented in the model because ice water content is nearly zero in the 50th percentile of the observed anvils as well as in most of the modeled anvils. In simulated medium and thick anvils, heating generally occurs too close to cloud top in schemes with the lowest ice content. In simulated thick anvils, the magnitude of longwave cooling near the tops of thick anvils is well treated in most simulations; however, too little cooling occurs throughout much of the rest of the cloud, and all simulations fail to replicate longwave warming near cloud base. Additionally, current radiation schemes in WRF do not incorporate newly available, but important, hydrometeor number concentrations. As two-moment microphysics schemes improve, radiation schemes must be updated to include such information because hydrometeor size distributions impact in-cloud heating.

Different microphysical schemes can produce vastly different representations of MCSs and their anvil cloud. Of six schemes tested, the one-moment Goddard scheme and the hybrid WDM6, which uses a single-moment approach for the ice phase, appear to outperform the schemes that use two moments in the ice-phase microphysics. These two schemes produce reasonable amounts of ice at the appropriate altitudes within anvils. The Goddard scheme even generates a robust representation of a midlevel thin cloud layer around 6–7 km. The schemes that use a double-moment approach for ice underproduce cloud ice and/or overproduce larger

precipitating ice and snow. Recall that our stringent method for testing microphysical schemes requires that each scheme produce a realistic amount of snow and ice at many different heights and that they generate correct relative fractions of thin, medium, and thick anvil. Therefore, we should not be surprised that each microphysical scheme does not satisfy our validation criteria. Satisfactory representation of anvil cloud by even two of the schemes tested is indicative of the recent advances made in microphysical parameterization of tropical convective cloudiness.

As seen in previous studies, all of the microphysical schemes produce too little cloud ice in thin anvil, resulting in clouds that are too optically thin. Additionally, the Milbrandt, Morrison, SBU-YLIN, and Thompson schemes fail to produce enough thin anvil relative to other anvil types. However, the Goddard and WDM6 schemes generate accurate relative proportions of thin, medium, and thick anvil. That thin anvils are generally poorly represented in the model is of great importance since they account for about two-thirds of the area covered by all MCS anvils. Consequently, their misrepresentation in models could significantly affect the net radiative heating simulated in the upper troposphere. In addition, even more abundant subvisible cirrus left behind by MCS anvil after the system dissipates has properties similar to that of thin anvil (not shown).

Results of this and similar studies can be used as insight regarding what improvements to make in parameterizations of microphysical processes. Treatment of aerosols as cloud condensation nuclei as well as adjustments in intercept parameters, densities, and fallout velocities of frozen hydrometeors will be investigated in future studies. Also, the general success attained in representing the basic radiative heating profile in anvil clouds and associated uncertainty gives us a basis for making initial global estimates of impacts by anvil clouds on the large-scale general circulation and climate by applying such profiles to the global distribution of MCSs determined from satellite data (e.g., Yuan and Houze 2010). The present results, however, apply to continental tropical anvils; oceanic anvil clouds differ in size and interior structure from continental anvils (Yuan et al. 2011). An important next step involves using radar data on oceanic tropical anvil clouds, such as that obtained from the ARM Madden-Julian oscillation Investigation Experiment and the Dynamics of the Madden-Julian Oscillation Field Project over the Indian Ocean. These new data will allow empirical information on radiation profiles and hydrometeor contents of oceanic anvils to be developed and models to be tested for their representations of anvil clouds over an oceanic domain.

Acknowledgments. This work was supported by DOE Grant DE-SC0001164/ER-64752. Stacy Brodzik provided technical support and data management. Beth Tully provided graphics and editorial assistance. The authors thank Alain Protat and two anonymous reviewers for their constructive comments on the manuscript.

REFERENCES

- Aspliden, C. I., Y. Tourre, and J. B. Sabine, 1976: Some climatological aspects of West African disturbance lines during GATE. *Mon. Wea. Rev.*, **104**, 1029–1035.
- Blossey, P. N., C. S. Bretherton, J. Cetrone, and M. Kharoutdinov, 2007: Cloud-resolving model simulations in KWAJEX: Model sensitivities and comparisons with satellite and radar observations. *J. Atmos. Sci.*, **64**, 1488–1508.
- Cetrone, J., and R. A. Houze Jr., 2009: Anvil clouds of tropical mesoscale convective systems in monsoon regions. *Quart. J. Roy. Meteor. Soc.*, **135**, 305–317.
- , and —, 2011: Leading and trailing anvil clouds of West African squall lines. *J. Atmos. Sci.*, **68**, 1114–1123.
- Chong, M., 2010: The 11 August 2006 squall-line system as observed from MIT Doppler radar during the AMMA SOP. *Quart. J. Roy. Meteor. Soc.*, **136** (S1), 209–226.
- , P. Amayenc, G. Scialom, and J. Testud, 1987: A tropical squall line observed during the COPT81 experiment in West Africa. Part I: Kinematic structure inferred from dual-Doppler radar data. *Mon. Wea. Rev.*, **115**, 670–694.
- Clement, A. C., and B. Soden, 2005: The sensitivity of the tropical-mean radiation budget. *J. Climate*, **18**, 3189–3203.
- Dudhia, J., 1989: Numerical study of convection observed during the winter monsoon experiment using a mesoscale two-dimensional model. *J. Atmos. Sci.*, **46**, 3077–3107.
- Dufresne, J.-L., and S. Bony, 2008: An assessment of the primary sources of spread of global warming estimates from coupled atmosphere–ocean models. *J. Climate*, **21**, 5135–5144.
- Ek, M. B., K. E. Mitchell, Y. Lin, E. Rogers, P. Grunmann, V. Koren, G. Gayno, and J. D. Tarpley, 2003: Implementation of Noah land surface model advances in the National Centers for Environmental Prediction operational mesoscale Eta model. *J. Geophys. Res.*, **108**, 8851, doi:10.1029/2002JD003296.
- Fink, A. H., and A. Reiner, 2003: Spatiotemporal variability of the relation between African easterly waves and West African squall lines in 1998 and 1999. *J. Geophys. Res.*, **108**, 4332, doi:10.1029/2002JD002816.
- Fortune, M., 1980: Properties of African squall lines inferred from time-lapse satellite imagery. *Mon. Wea. Rev.*, **108**, 153–168.
- Frey, W., and Coauthors, 2011: In situ measurements of tropical cloud properties in the West African monsoon: Upper tropospheric ice clouds, mesoscale convective system outflow, and subvisual cirrus. *Atmos. Chem. Phys.*, **11**, 5569–5590.
- Fu, Q., 1996: An accurate parameterization of the solar radiative properties of cirrus clouds for climate models. *J. Climate*, **9**, 2058–2082.
- , and K. N. Liou, 1992: On the correlated k -distribution method for radiative transfer in nonhomogeneous atmospheres. *J. Atmos. Sci.*, **49**, 2139–2156.
- , P. Yang, and W. B. Sun, 1998: An accurate parameterization of the infrared radiative properties of cirrus clouds for climate models. *J. Climate*, **11**, 2223–2237.

- Futyan, J., and A. Del Genio, 2007: Deep convective system evolution over Africa and the tropical Atlantic. *J. Climate*, **20**, 5041–4060.
- Hamilton, R. A., and J. W. Archibold, 1945: Meteorology of Nigeria and adjacent territory. *Quart. J. Roy. Meteor. Soc.*, **71**, 231–264.
- Hartmann, D. L., H. H. Hendon, and R. A. Houze Jr., 1984: Some implications of the mesoscale circulations in tropical cloud clusters for large-scale dynamics and climate. *J. Atmos. Sci.*, **41**, 113–121.
- Hong, G., 2007: Radar backscattering properties of nonspherical ice crystals at 94 GHz. *J. Geophys. Res.*, **112**, D22203, doi:10.1029/2007JD008839.
- Hong, S.-Y., Y. Noh, and J. Dudhia, 2006: A new vertical diffusion package with an explicit treatment of entrainment processes. *Mon. Wea. Rev.*, **134**, 2318–2341.
- Houze, R. A., Jr., 1982: Cloud clusters and large-scale vertical motions in the tropics. *J. Meteor. Soc. Japan*, **60**, 396–410.
- , 2004: Mesoscale convective systems. *Rev. Geophys.*, **42**, RG4003, doi:10.1029/2004RG000150.
- , S. A. Rutledge, M. I. Biggerstaff, and B. F. Smull, 1989: Interpretation of Doppler weather radar displays of midlatitude mesoscale convective systems. *Bull. Amer. Meteor. Soc.*, **70**, 608–619.
- Iacono, M. J., E. L. Mlawer, S. A. Clough, and J. J. Morcrette, 2000: Impact of an improved longwave radiation model, RRTM, on the energy budget and thermodynamic properties of the NCAR Community Climate Model, CCM3. *J. Geophys. Res.*, **105** (D11), 14 873–14 890.
- Johnson, R. H., T. M. Rickenbach, S. A. Rutledge, P. E. Ciesielski, and W. H. Schubert, 1999: Trimodal characteristics of tropical convection. *J. Climate*, **12**, 2397–2418.
- Kain, J. S., 2004: The Kain–Fritsch convective parameterization: An update. *J. Appl. Meteor.*, **43**, 170–181.
- Kulie, M. S., R. Bennartz, T. J. Greenwald, Y. Chen, and F. Weng, 2010: Uncertainties in microwave properties of frozen precipitation: Implications for remote sensing and data assimilation. *J. Atmos. Sci.*, **67**, 3471–3487.
- Lang, S., W.-K. Tao, R. Cifelli, W. Olson, J. Halverson, S. Rutledge, and J. Simpson, 2007: Improving simulations of convective systems from TRMM LBA: Easterly and westerly regimes. *J. Atmos. Sci.*, **64**, 1141–1164.
- Liebe, H. J., 1985: An updated model for millimeter wave propagation in moist air. *Radio Sci.*, **20**, 1069–1089.
- Lim, K.-S. S., and S.-Y. Hong, 2010: Development of an effective double-moment cloud microphysics scheme with prognostic cloud condensation nuclei (CCN) for weather and climate models. *Mon. Wea. Rev.*, **138**, 1587–1612.
- Lin, J., B. Mapes, M. Zhang, and M. Newman, 2004: Stratiform precipitation, vertical heating profiles, and the Madden–Julian oscillation. *J. Atmos. Sci.*, **61**, 296–309.
- Lin, Y., and B. A. Colle, 2011: A new bulk microphysical scheme that includes riming intensity and temperature-dependent ice characteristics. *Mon. Wea. Rev.*, **139**, 1013–1035.
- , L. J. Donner, and B. A. Colle, 2011: Parameterization of riming intensity and its impact on ice fall speed using ARM data. *Mon. Wea. Rev.*, **139**, 1036–1047.
- Lin, Y.-L., R. D. Farley, and H. D. Orville, 1983: Bulk parameterization of the snow field in a cloud model. *J. Climate Appl. Meteor.*, **22**, 1065–1092.
- Lopez, M. A., D. L. Hartmann, P. N. Blossey, R. Wood, C. S. Bretherton, and T. L. Kubar, 2009: A test of the simulation of tropical convective cloudiness by a cloud-resolving model. *J. Climate*, **22**, 2834–2849.
- Masunaga, H., and Coauthors, 2010: Satellite Data Simulator Unit: A multisensor, multispectral satellite simulator package. *Bull. Amer. Meteor. Soc.*, **91**, 1625–1632.
- Mather, J. H., S. A. McFarlane, M. A. Miller, and K. L. Johnson, 2007: Cloud properties and associated radiative heating rates in the tropical western Pacific. *J. Geophys. Res.*, **112**, D05201, doi:10.1029/2006JD007555.
- Matsui, T. M., X. Zeng, W.-K. Tao, H. Masunaga, W. S. Olson, and S. Lang, 2009: Evaluation of long-term cloud-resolving model simulations using satellite radiance observations and multifrequency satellite simulators. *J. Atmos. Oceanic Technol.*, **26**, 1261–1274.
- McFarlane, S. A., J. H. Mather, and T. P. Ackerman, 2007: Analysis of tropical radiative heating profiles: A comparison of models and observations. *J. Geophys. Res.*, **112**, D14218, doi:10.1029/2006JD008290.
- Mead, J. B., and K. B. Widener, 2005: W-band ARM cloud radar. Preprints, *32nd Conf. on Radar Meteorology*, Albuquerque, NM, Amer. Meteor. Soc., P1R.3. [Available online at <http://ams.confex.com/ams/pdfpapers/95978.pdf>.]
- Milbrandt, J. A., and M. K. Yau, 2005: A multimoment bulk microphysics parameterization. Part II: A proposed three-moment closure and scheme description. *J. Atmos. Sci.*, **62**, 3065–3081.
- Mlawer, E. J., S. J. Taubman, P. D. Brown, M. J. Iacono, and S. A. Cough, 1997: Radiative transfer for inhomogeneous atmospheres: RRTM, a validated correlated-*k* model for the longwave. *J. Geophys. Res.*, **102** (D14), 16 663–16 682.
- Morris, V. M., 2006: Microwave Radiometer (MWR) Handbook. ARM-TR016, 20 pp. [Available online at http://www.wmo.int/pages/prog/gcos/documents/gruanmanuals/Z_instruments/mwr_handbook.pdf.]
- Morrison, H., G. Thompson, and V. Tatarskii, 2009: Impact of cloud microphysics on the development of trailing stratiform precipitation in a simulated squall line: Comparison of one- and two-moment schemes. *Mon. Wea. Rev.*, **137**, 991–1007.
- Noh, Y., W.-G. Cheon, S.-Y. Hong, and S. Raasch, 2003: Improvement of the K-profile model for the planetary boundary layer based on large eddy simulation data. *Bound.-Layer Meteorol.*, **107**, 401–427.
- Protat, A., J. Delanoe, D. Bouniol, A. J. Heymsfield, A. Bansemmer, and P. Brown, 2007: Evaluation of ice water content retrievals from cloud radar reflectivity and temperature using a large airborne in situ microphysical database. *J. Appl. Meteor. Climatol.*, **46**, 557–572.
- , —, A. Plana-Fattori, P. T. May, and E. J. O’Connor, 2010: The statistical properties of tropical ice clouds generated by the West African and Australian monsoons, from ground-based radar–lidar observations. *Quart. J. Roy. Meteor. Soc.*, **136** (S1), 345–363.
- Redelsperger, J.-L., C. D. Thorncroft, A. Diedhiou, T. Lebel, D. J. Parker, and J. Polcher, 2006: African Monsoon Multi-disciplinary Analysis: An international research project and field campaign. *Bull. Amer. Meteor. Soc.*, **87**, 1739–1746.
- Rutledge, S. A., and P. V. Hobbs, 1984: The mesoscale and microscale structure and organization of clouds and precipitation in midlatitude cyclones. XII: A diagnostic modeling of study of precipitation development in narrow cold-frontal rainbands. *J. Atmos. Sci.*, **41**, 2949–2972.
- Schumacher, C., and R. A. Houze Jr., 2006: Stratiform precipitation production over sub-Saharan Africa and the tropical east Atlantic as observed by TRMM. *Quart. J. Roy. Meteor. Soc.*, **132**, 2235–2255.

- , —, and I. Kraucunas, 2004: The tropical dynamical response to latent heating estimates derived from the TRMM precipitation radar. *J. Atmos. Sci.*, **61**, 1341–1358.
- Skamarock, W. C., and Coauthors, 2008: A description of the Advanced Research WRF version 3. NCAR Tech. Note NCAR/TN- 475+STR, 125 pp. [Available online at http://www.mmm.ucar.edu/wrf/users/docs/arw_v3.pdf.]
- Solomon, S., D. Qin, M. Manning, M. Marquis, K. Averyt, M. M. B. Tignor, L. Miller Jr., and Z. Chen, Eds., 2007: *Climate Change 2007: The Physical Science Basis*. Cambridge University Press, 996 pp.
- Tao, W.-K., J. Simpson, and M. McCumber, 1989: An ice-water saturation adjustment. *Mon. Wea. Rev.*, **117**, 231–235.
- Thompson, G., P. R. Field, R. M. Rasmussen, and W. D. Hall, 2008: Explicit forecasts of winter precipitation using an improved bulk microphysics scheme. Part II: Implementation of a new snow parameterization. *Mon. Wea. Rev.*, **136**, 5095–5115.
- Troyan, D., 2012: Merged sounding value-added product. U.S. Department of Energy Rep. DOE/SC-ARM/TR-087, 19 pp. [Available online at http://www.arm.gov/publications/tech_reports/doe-sc-arm-tr-087.pdf.]
- Wang, Z., and K. Sassen, 2002: Cirrus cloud microphysical property retrieval using lidar and radar measurements. Part I: Algorithm description and comparison with in situ data. *J. Appl. Meteor.*, **41**, 218–229.
- Webster, P. J., and G. L. Stephens, 1980: Tropical upper-tropospheric extended clouds: Inferences from winter MONEX. *J. Atmos. Sci.*, **37**, 1521–1541.
- Yuan, J., and D. L. Hartmann, 2008: Spatial and temporal dependence of clouds and their radiative impacts on the large-scale vertical velocity profile. *J. Geophys. Res.*, **113**, D19201, doi:10.1029/2007JD009722.
- , and R. A. Houze Jr., 2010: Global variability of mesoscale convective system anvil structure from A-train satellite data. *J. Climate*, **23**, 5864–5888.
- , —, and A. Heymsfield, 2011: Vertical structures of anvil clouds of tropical mesoscale convective systems observed by *CloudSat*. *J. Atmos. Sci.*, **68**, 1653–1674.
- Yuter, S. E., and R. A. Houze Jr., 1995: Three-dimensional kinematic and microphysical evolution of Florida cumulonimbus. Part II: Frequency distribution of vertical velocity, reflectivity, and differential reflectivity. *Mon. Wea. Rev.*, **123**, 1941–1963.
- Zeng, X., W.-K. Tao, S. Lang, A. Y. Hou, M. Zhang, and J. Simpson, 2008: On the sensitivity of atmospheric ensembles to cloud microphysics in long-term cloud-resolving model simulations. *J. Meteor. Soc. Japan*, **86A**, 45–65.